

Langmuir–Blodgett Fabrication of Two-Dimensional Robust Cross-Linked Nanoparticle Assemblies

Shaowei Chen*

Department of Chemistry, Southern Illinois University, Carbondale, Illinois 62901

Received December 11, 2000. In Final Form: February 19, 2001

Two-dimensional nanoparticle cross-linked networks were constructed by using the Langmuir–Blodgett technique, where neighboring particles were chemically bridged by bifunctional linkers at the air/water interface. The cross-linking process was effected at high surface pressures by ligand intercalation and surface exchange reactions between the bifunctional linkers (rigid aryl dithiols) and the particle-bound alkanethiolates, resulting in the formation of long-range ordered and robust particle superlattice networks. Even for particles with varied thicknesses of the protecting monolayers, effective cross-linking was achieved where the interparticle spacing appeared to be determined by the molecular length of the bifunctional linkers. One of the potential applications of the resulting particle networks is for the construction of two-dimensional quantum dot arrays by ultraviolet and ozone molecular cleaning, where the organic components were removed rather efficiently leaving the metal particles deposited onto the substrate surface. This could be used for efficient large-scale surface nanofabrication in a nonlithographic manner.

Introduction

The recent intense research interest in nanosized particle materials has been largely driven by the technological implication of these novel structural elements in the “nano-aturizations” of optical, electronic, and magnetic devices.^{1,2} One of the technical challenges in the “bottom-up” approach³ in the construction of these nanoscale entities is to develop efficient methods to organize nanoparticles into ordered and robust arrays in a controllable manner, where the collective properties of the particle assemblies can be easily manipulated by the nature and composition of the particles as well as the physical distribution of the particles in the ensembles. In particular, much research effort has been focused on the construction of two-dimensional organized assemblies that can serve as the structural basis for more complicated nanostructures. Several approaches have been reported. For instance, nanoparticles of narrow dispersity can self-organize into ordered structures by simply drop-casting the particle solution onto a substrate.⁴ However, the particle assemblies generally lack long-range ordering and good reproducibility. Another approach relies on bifunctional ligands that immobilize the particles to a substrate surface by a sequential anchoring mechanism.^{5,6} Further improvement is made by first incorporating the bifunctional linkers into the nanoparticle surface rendering the particles surface-active with peripheral anchoring groups,

which can then be self-assembled onto substrate surfaces, akin to monomeric alkanethiol molecules.⁷ This self-assembling approach is very effective in achieving particle assemblies of high surface coverage and, thanks to the strong chemical interactions between the anchor sites and the substrate (and, hence, a “vertical” approach), leads to the fabrications of mechanically robust particle structures. Apparently, the latter is the limiting factor in the application of this route. In the case that the interactions between the particles and the substrate are weak, equally stable particle network structures can be constructed by using the Langmuir–Blodgett (LB) technique (a “horizontal” approach), where neighboring particles were cross-linked by, again, bifunctional linkers at the air/water interface.⁸

It is a well-known procedure to use the LB technique to manipulate the molecular ordering of the nanoparticle thin films.^{9,10} However, the resulting particle assemblies typically lack long-term stability, in particular when deposited at relatively low surface pressures, mainly because of the relatively weak interactions between neighboring particles as well as between particles and substrates. By cross-linking the neighboring particles with strong chemical bridges, we aim at developing an effective method to construct particle ensembles with enhanced mechanical stability, which might ultimately lead to the fabrication of stand-alone nanoparticle thin films. Recently, we showed that nanoparticle cross-linking could

* Fax: 618-453-6408. E-mail: schen@chem.siu.edu.

(1) (a) Schmid, G. *Clusters and Colloids: From Theory to Applications*; VCH: New York, 1994. (b) Turtton, R. *The Quantum Dot: A Journey into the Future of Microelectronics*; Oxford University Press: New York, 1995.

(2) See also all the review articles in the Feb 16, 1996 and November 24, 2000 issues of *Science*.

(3) See, for instance, the Special Reports in the October 16, 2000 issue of *Chem. Eng. News*.

(4) (a) Sun, S.; Murray, C. B.; Weller, D.; Folks, L.; Moser, A. *Science* **2000**, *287*, 1989. (b) Kiely, C. J.; Fink, J.; Brust, M.; Bethell, D.; Schiffrin, D. J. *Nature* **1998**, *396*, 444. (c) Wang, Z. L. *Adv. Mater.* **1998**, *10*, 13. (d) Pileni, M.-P. *New J. Chem.* **1998**, 693. (e) Whetten, R. L.; Khoury, J. T.; Alvarez, M. M.; Murthy, S.; Vezmar, I.; Wang, Z. L.; Stephens, P. W.; Cleveland, C. L.; Luetke, W. D.; Landman, U. *Adv. Mater.* **1996**, *8*, 428. (f) Murray, C. B.; Kagan, C. R.; Bawendi, M. G. *Science* **1995**, *270*, 1335. (g) Osifchin, R. G.; Andres, R. P.; Henderson, J. I.; Kubiak, C. P.; Dominey, R. N. *Nanotechnology* **1996**, *7*, 412.

(5) (a) Schmid, G. *J. Chem. Soc., Dalton Trans.* **1998**, 1077. (b) Andres, R. P.; Bielefeld, J. D.; Henderson, J. I.; Janes, D. B.; Kolagunta, V. R.; Kubiak, C. P.; Mahoney, W. J.; Osifchin, R. G. *Science* **1996**, *273*, 1690. (c) Feldheim, D. L.; Grabar, K. C.; Natan, M. J.; Mallouk, T. E. *J. Am. Chem. Soc.* **1996**, *118*, 7640. (d) Taton, T. A.; Mucic, R. C.; Mirkin, C. A.; Letsinger, R. L. *J. Am. Chem. Soc.* **2000**, *122*, 6305. (e) Mann, S.; Shenton, W.; Li, M.; Connolly, S.; Fitzmaurice, D. *Adv. Mater.* **2000**, *12*, 147.

(6) (a) Feldheim, D. L.; Keating, C. D. *Chem. Soc. Rev.* **1998**, *1*, 27. (b) Collier, C. P.; Vossmeier, T.; Heath, J. R. *Annu. Rev. Phys. Chem.* **1998**, *49*, 371.

(7) (a) Chen, S. *J. Phys. Chem. B* **2000**, *104*, 663. (b) Chen, S. *J. Am. Chem. Soc.* **2000**, *122*, 7420.

(8) Chen, S. *Adv. Mater.* **2000**, *12*, 186.

(9) (a) Collier, C. P.; Saykally, R. J.; Shiang, J. J.; Henrichs, S. E.; Heath, J. R. *Science* **1997**, *277*, 1978. (b) Yi, K. C.; Hórvölgyi, Z.; Fendler, J. H. *J. Phys. Chem.* **1994**, *98*, 3872.

(10) Lee, W.-Y.; Hostetler, M. J.; Murray, R. W.; Majda, M. *Isr. J. Chem.* **1997**, *37*, 213.

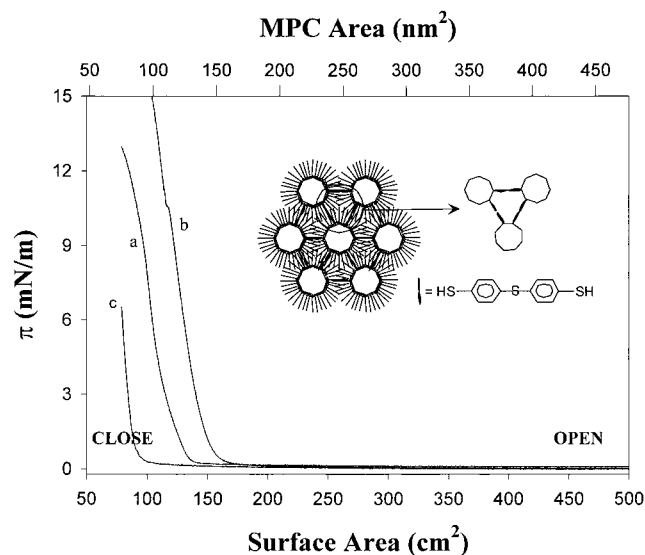


Figure 1. LB isotherms of C8Au particles before and after TBBT cross-linking. Initially, 150 μL of the C8Au particle solution in hexane (1 mg/mL) was spread onto the water surface. The TBBT concentration was 4 mM in CH_2Cl_2 , and 75 μL was added to the water surface. (a) is the isotherm of the C8Au particles prior to the addition of TBBT; (b) is the first compression after the introduction of TBBT; (c) is the isotherm of the resulting particle networks after holding the barrier in the closed position for 15 h. The inset shows the schematic of the particle cross-linked networks.

be initiated at high surface pressures by confining the particles and the cross-linking reagents on the water surface, where robust and compact particle networks were readily constructed.⁸ In addition, the networking between neighboring particles at the air/water interface has been demonstrated by, for instance, the cross-linking of aminoethanethiol-modified CdS semiconductor nanoparticles by glutaraldehyde in the *subphase*, where the resulting particle networks exhibited enhanced n-type photosensitivity.¹¹

One of the intriguing potential applications of these robust nanoparticle assemblies lies in the construction of surface nanostructures where long-range (metal) quantum dot arrays can be readily fabricated in a nonlithographic manner. Here, the organic components can be removed photochemically, leaving the quantum dots deposited onto the substrate surfaces. As the nanodot dimensions are mainly determined by the original particle sizes, this nanoparticle-based approach might serve as a complementary route to other surface fabrication techniques where nanometer-sized patterning remains a challenge. For instance, in nanosphere lithography¹² close-packed micrometer-sized colloidal particles are used as the masking template and metal islands are grown in the particle interstices, with a dimension as big as a few tenths of the colloid radius. In addition, it is anticipated that the surface quantum dot arrays will provide a well-defined structural basis for surface nanoscale chemical functionalization that might not be readily accessible by other methods (e.g., microcontact printing¹³ or scanning probe microscopy based surface nanografting¹⁴).

In our previous report,⁸ we demonstrated that alkanethiolate-protected gold nanoparticles could be net-

worked by rigid aryldithiol linkers (e.g., 4,4'-thiobisbenzenethiol, TBBT) at relatively high surface pressures, as evidenced by optical and electron microscopic measurements. Dithiols have been used previously to cross-link gold particles, forming three-dimensional aggregates where the dithiol ligands were introduced into the particle-protecting monolayers, and upon the removal of solvents this assembling process occurred rather quickly, efficiently, and yet uncontrollably.¹⁵ To use dithiols as the linkers to achieve two-dimensional cross-linked nanoparticle networks, we brought the particles and the rigid dithiol linkers into contact at the air/water interface, where the cross-linking process was confined to the interfacial region and initiated at relatively high surface pressure presumably because of ligand intercalation and surface place-exchange reactions.^{16c}

However, the resulting particle networks⁸ did not show an ordered superlattice structure, which was ascribed to the modest dispersivity of the particles. In this report, we carry out further studies using rather monodisperse particles, where long-range ordered and robust particle superlattice assemblies are obtained. The effect of the particle-protecting monolayers will also be investigated by using particles of varied monolayer thicknesses. In addition, we will present some preliminary studies of using these particle networks as the structural basis for surface nonlithographic fabrication.

Experimental Section

Materials. $\text{HAuCl}_4 \cdot x\text{H}_2\text{O}$ (Aldrich), 1-hexanethiol (C6SH, 96%, ACROS), 1-octanethiol (C8SH, 97%, ACROS), 1-decanethiol (C10SH, 96%, ACROS), 1-dodecanethiol (C12SH, 98%, ACROS), and 4,4'-thiobisbenzenethiol (TBBT, Aldrich) were all used as received. Water was supplied by a Barnstead Nanopure water system (18.3 M Ω). All other solvents were obtained from typical commercial sources and used without further purification.

Alkanethiolate-protected gold nanoparticles were synthesized by using the Brust route.¹⁶ These particles were then dissolved in a toluene solution and under thermal annealing at 140 $^\circ\text{C}$ using an oil bath for about 8 h.¹⁷ The resulting particles showed a much narrower size dispersity and a mostly spherical shape. In this study, four samples were used: C6Au, C8Au, C10Au, and C12Au, which denote the gold nanoparticles protected by a monolayer of C6SH, C8SH, C10SH, and C12SH, respectively. Their core sizes were estimated to be 5.1, 4.7, 5.2, and 5.1 nm, respectively, as determined by transmission electron microscopic measurements (see below), with all size dispersities less than 5%.

Nanoparticle Thin Films. Nanoparticle cross-linked networks were fabricated at the air/water interface using a Langmuir-Blodgett trough (NIMA model 611) with a Wilhelmy plate as the surface-pressure sensor and Nanopure water as the subphase. The details have been described previously.⁸ In a typical experiment, the particle solutions were prepared in hexane at a concentration of 1 mg/mL (ca. 1 μM). An aliquot of 100–200 μL was then spread slowly onto the water surface in a dropwise fashion using a Hamilton microliter syringe. Nanoparticle cross-linking was initiated at high surface pressures after the introduction of bifunctional TBBT ligands (typically 50 μL of 4 mM TBBT solution in CH_2Cl_2 was spread onto the water surface with the barrier at the open (500 cm^2) position). At least 20 min

(13) Xia, Y.; Mrksich, M.; Kim, E.; Whitesides, G. M. *J. Am. Chem. Soc.* **1995**, *117*, 9576.

(14) Liu, G.-Y.; Xu, S.; Qian, Y. *Acc. Chem. Res.* **2000**, *33*, 457.

(15) Brust, M.; Bethell, D.; Schiffrin, D. J.; Kiely, C. J. *Adv. Mater.* **1995**, *7*, 795.

(16) (a) Brust, M.; Walker, M.; Bethell, D.; Schiffrin, D. J.; Kiely, R. *J. Chem. Soc., Chem. Commun.* **1994**, 801. (b) Whetten, R. L.; Shafiqullin, M. N.; Khoury, J. T.; Schaaff, T. G.; Vezmar, I.; Alvarez, M. M.; Wilkinson, A. *Acc. Chem. Res.* **1999**, *32*, 397. (c) Templeton, A. C.; Wuelfing, W. P.; Murray, R. W. *Acc. Chem. Res.* **2000**, *33*, 27.

(17) Maye, M. M.; Zheng, W.; Leibowitz, F. L.; Ly, N. K.; Zhong, C.-J. *Langmuir* **2000**, *16*, 490.

(11) Torimoto, T.; Tsumura, N.; Miyake, M.; Nishizawa, M.; Sakata, T.; Mori, H.; Yoneyama, H. *Langmuir* **1999**, *15*, 1853.

(12) (a) Boneberg, J.; Burmeister, F.; Schäfle, C.; Leiderer, P.; Reim, D.; Fery, A.; Herminghaus, S. *Langmuir* **1997**, *13*, 7080. (b) Jensen, T. R.; Duval, M. L.; Kelly, K. L.; Lazarides, A. A.; Schatz, G. C.; van Duyne, R. P. *J. Phys. Chem. B* **1999**, *103*, 9846.

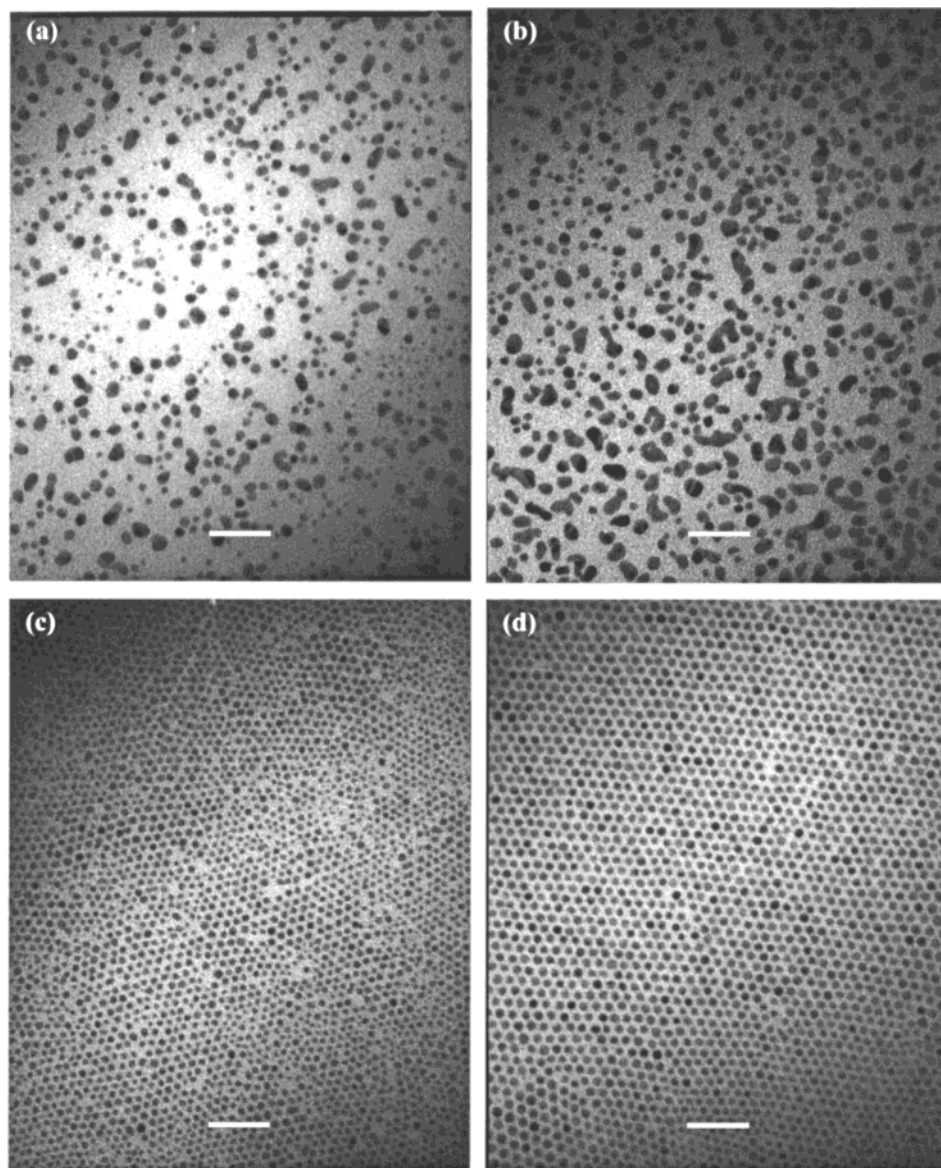


Figure 2. TEM micrographs of the C8Au particles deposited onto a SiO_x-coated Cu grid at varied surface pressures before and after TBBT cross-linking (details in Figure 1): (a) no TBBT, 4 mN/m; (b) no TBBT, 7 mN/m; (c) after TBBT networking, 4 mN/m; (d) after TBBT networking, 7 mN/m. The scale bars are all 33 nm.

was allowed for solvent evaporation prior to isotherm measurements and between compression cycles. The barrier moving speed was 20 cm²/min.

Particle monolayers were deposited onto SiO_x-coated Cu grids and ultraviolet–ozone (UVO)-cleaned glass slides (15 min, UVO Cleaner model 42, Jelight Co.) by lifting the substrates vertically under controlled surface pressures at a speed of 1 mm/min. The transmission electron microscope grids were used as received (from SPI) and placed onto a glass slide surface to ensure that only one face of the grid is deposited with the particle monolayers. The samples were then subjected to optical and electron microscopic characterizations, before and after subsequent UVO exposure.

Transmission Electron Microscopy (TEM). TEM measurements were carried out with a Hitachi 7100 transmission electron microscope at 100 kV, which was also equipped with a Noran Voyager III energy-dispersive X-ray (EDX) detector. Phase-contrast micrographs were captured at 300–500K magnification.

UV–Vis Spectroscopy. UV–vis spectra were acquired with an ATI Unicam UV4 spectrometer with a resolution of 2 nm. The spectra were normalized to their respective absorption intensity at 272 nm. For particles dissolved in hexane, the particle concentration was generally about 0.1 mg/mL.

Results and Discussion

Here, we start with an investigation of the formation of nanoparticle cross-linked networks at the air/water interface by using the Langmuir–Blodgett method, followed by a study of the chain length effect of the particle-protecting monolayers and a preliminary study of using these robust particle patches as the structural basis for surface nanofabrication in a nonlithographic manner.

Nanoparticle Networking. The formation of nanoparticle networks is achieved by using the Langmuir–Blodgett method, where interparticle cross-linking is initiated on the water surface at relatively high surface pressures (e.g., 7 mN/m) in the presence of rigid bifunctional ligands (e.g., aryl dithiols).⁸ This is ascribed to ligand intercalation and hence surface exchange reactions between the linking reagents and the particle-bound thiolates. The networking process can be manifested by monitoring the variation of the surface isotherms. Figure 1 shows the isotherms of C8Au particles before (a) and after (b) the addition of TBBT. One can see that both

isotherms show rather similar rising slopes, indicating a similarity of the compressibility in these two cases. However, when the barrier is held at the closed position for about 15 h, the subsequent compression shows an isotherm (c) that is vastly different from the previous two (a and b): (i) the takeoff area is even much smaller than that prior to the addition of TBBT (a) and (ii) the rising slope is much steeper. Both observations indicate a more rigid and compact nature of the particle thin films on the water surface and strongly suggest the formation of nanoparticle cross-linked networks (Figure 1 inset). In fact, one can see that on the water surface, macroscale purple particle patches are very visible, whereas the original particle thin films without the addition of TBBT look brown/pink (vide infra). These particle patches were very stable, virtually unchanged for days even with the barrier at the open position.

The formation of nanoparticle networks is further supported by more direct and visual characterizations, such as TEM measurements. Figure 2 shows the TEM micrographs of the C8Au particles deposited onto SiO_x-coated Cu grids at varied surface pressures prior to the addition of TBBT (a and b) as well as after holding the barrier at the closed position in the presence of TBBT (c and d). One can see that in the original particle thin films without TBBT (a and b), only rather random distribution of the particles is observed; in addition, there appears to be some particle coalescence forming twins or higher-order oligomers of the particles. In sharp contrast, after the particles were compressed with added TBBT molecules, the resulting particle assemblies show striking long-range ordered structures (c and d), where it can be clearly seen that rather close-packed superlattices are formed without the appearance of particle aggregation (defects are relatively rare and generally observed near particles that are not uniform in size, e.g., Figure 2c).

It should also be noted that the deposition pressure appears not to be an important factor in controlling the interparticle spacing once the particles are cross-linked by TBBT ligands. For instance, in both (c) and (d) where the particles were deposited at 4 and 7 mN/m, respectively, the interparticle spacing is found for both at ca. 1.6 nm. By taking into account the Au–S bond length, this spacing is very close to a single molecular length of TBBT (the molecular length of TBBT is 1.2 nm, as calculated by Hyperchem). In contrast, without the bridging ligands the particle spacing (and hence particle density) is predictably varied with surface pressure, as shown in Figure 2a,b.

Optical characterization provides further evidence of the formation of particle cross-linked networks. Figure 3 (top panel) shows the UV–vis spectra of the C8Au particles that were deposited onto clean glass slide surfaces at varied surface pressures before (a1 and b1) and after (c1 and d1) TBBT cross-linking. Also shown is the absorption spectrum of the particles dissolved in hexane (e). It is well-known that nanosized gold particles exhibit a unique surface-plasmon (SP) absorption band which is superimposed onto the exponential-decay Mie scattering profiles.^{16,18} The specific position of the SP band is very sensitive to the size, shape, and chemical environments of the particles (e.g., interparticle spacing),^{16c,18} a property that has been exploited as the sensing responses for chemical/biological identifications, for instance.¹⁹ Here, as anticipated, for the C8Au particles dissolved in solution, the SP band is

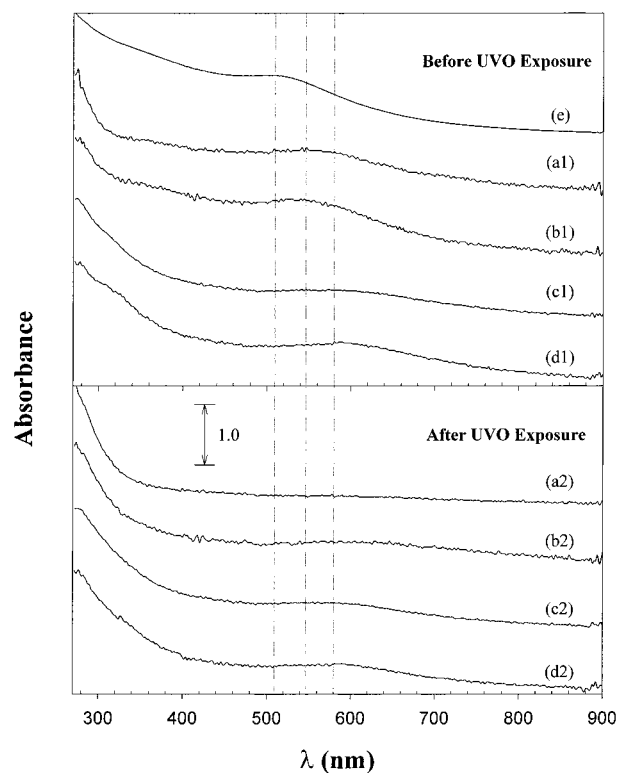


Figure 3. UV–vis spectra of the C8Au particle monolayers deposited onto cleaned glass slide surfaces at varied surface pressures before or after TBBT cross-linking (upper panel): (a1) no TBBT, $\pi = 4$ mN/m; (b1) no TBBT, $\pi = 7$ mN/m; (c1) TBBT added, $\pi = 4$ mN/m; (d1) TBBT added, $\pi = 7$ mN/m. Effects of UV–ozone exposure to the particle thin films are shown in the lower panel: (a2) to (d2) are the corresponding spectra of (a1) to (d1) after UV exposure, respectively. Also shown is the spectrum (e) of the C8Au particles dissolved in hexane (concentration ca. 0.1 mg/mL). All spectra were normalized to their respective absorbance at 272 nm and offset for the sake of clarity. Other experimental conditions are the same as in Figure 2.

found at ca. 510 nm (e). However, when the C8Au particle monolayers were deposited at 4 or 7 mN/m (a1 and b1, respectively) onto clean glass substrates (even without the cross-linking of TBBT), it can be seen that the corresponding absorption profiles are broadened and the SP band red-shifts to about 550 nm. When TBBT cross-linking is initiated, the red-shifting of the SP energy is even more pronounced, to 580 nm (c1 and d1, where the deposition pressures are 4 and 7 mN/m, respectively). These observations are consistent with the colorimetric change of the particle monolayers mentioned above as well as the interparticle spacing manifested by the TEM measurements (Figure 2), where the red-shifting is clearly due to the electronic coupling interactions between adjacent particles and increases with decreasing interparticle separation. Within the experimental context here, there is no significant variation of the SP energy with deposition pressures either before or after TBBT cross-linking.

These studies clearly demonstrate that the interparticle cross-linking can be effectively achieved at relatively high surface pressures by using bifunctional chemical bridges, leading to the formation of mechanically robust and long-range ordered nanoparticle superlattices.

Effects of Particle-Protecting Monolayers. As stipulated above, the interparticle cross-linking is effected by the intercalation and exchange reactions of bifunctional TBBT molecules with particle-protecting (alkanethiolate)

(18) Underwood, S.; Mulvaney, P. *Langmuir* **1994**, *10*, 3427.

(19) Mirkin, C. A.; Letsinger, R. L.; Mucic, R. C.; Storhoff, J. J. *Nature* **1996**, *382*, 607.

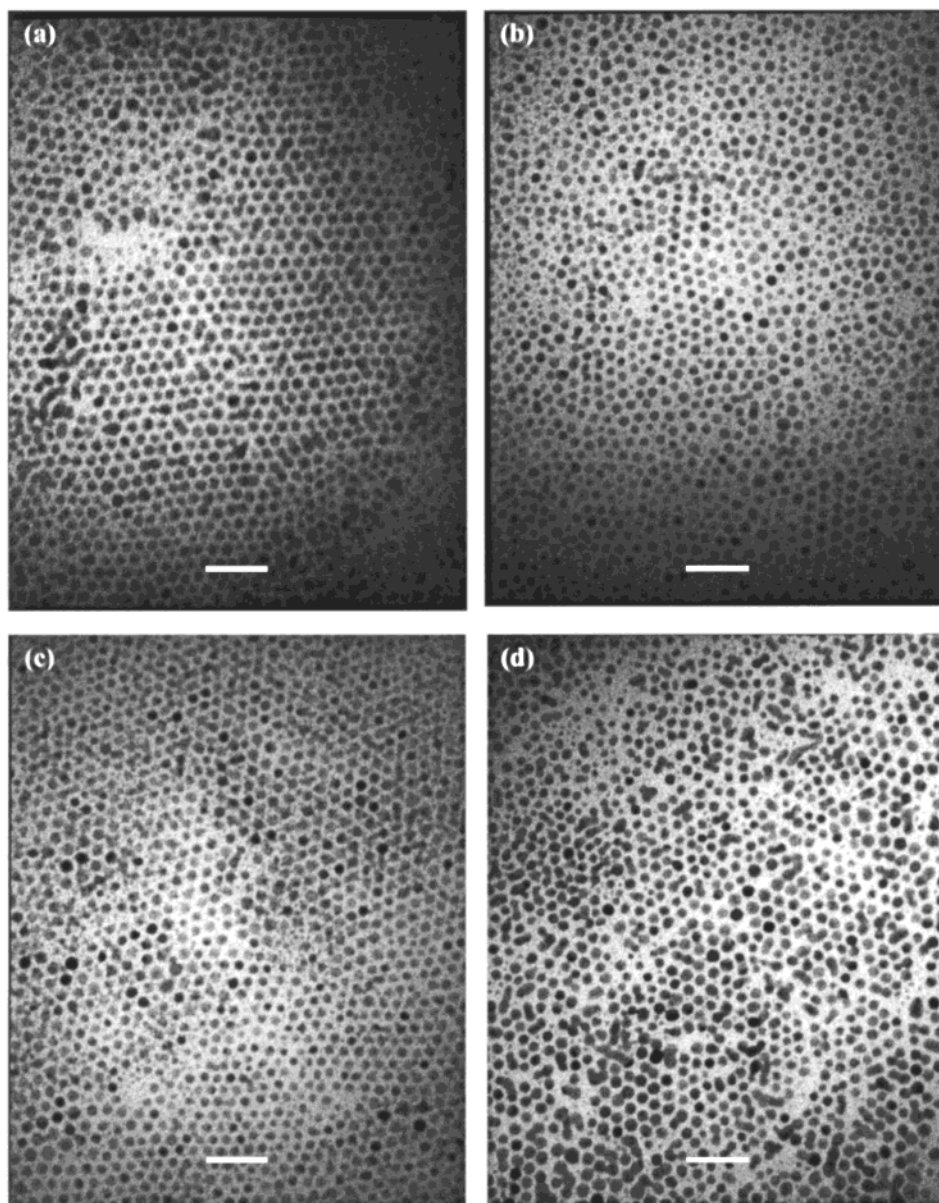


Figure 4. TEM micrographs of varied gold particle networks cross-linked by TBBT. (a) C6Au MPC, 200 μL spread, and TBBT 50 μL added. The particle film was deposited at 6 mN/m. (b) C10Au MPC, 100 μL spread, and TBBT 50 μL added. The particle film was deposited at 4 mN/m. (c) C12Au MPC, 100 μL spread, and TBBT 50 μL added. The particle film was deposited at 6 mN/m. (d) The same particle film as in (c) but treated with UV-ozone exposure for 15 min. All particle solutions were 1 mg/mL in hexane. The TBBT concentration was 4 mM. The scale bars are 20 nm in (a), 25 nm in (b), and 33 nm in both (c) and (d).

monolayers at high surface pressures. The above LB protocol was then used to fabricate robust cross-linked networks of gold nanoparticles with varied protecting monolayers. The LB isotherms observed in the formation of these varied particle networks are very similar to each other and to those shown in Figure 1 for C8Au particles (hence not shown). Again, large-scale purple particle patches were very visible on the water surface. Figure 4 shows the representative TEM micrographs of these particle assemblies that were originally protected by varied alkanethiolate monolayers: (a) 1-hexanethiolate (C6), (b) 1-decanethiolate (C10), and (c) 1-dodecanethiolate (C12). Despite the variation of the thickness of particle-protecting monolayers (C6, 0.78 nm; C8, 1.04 nm; C10, 1.29 nm; C12, 1.55 nm; all calculated by Hyperchem), the closest interparticle spacing is found to be ca. 1.6 nm in all these TBBT-bridged particle networks, which is equal to a single TBBT molecular length, as described earlier. Certainly, at the moment, it is hard to tell if all neighboring particles

are linked to each other. However, it is believed that interparticle networking is rampant enough to sustain the entire particle structures, with some disruptions at the defect sites that are largely ascribed to particle size dispersity. Although it might be somewhat surprising that for particles with protecting ligands longer than the chemical bridges (TBBT) the cross-linking is still achievable, it has been demonstrated previously that the organic shells of nanosized particles could be readily compressed.^{9a}

Additionally, the optical properties of these particle cross-linked networks exhibit similar responses in the UV-vis spectroscopic measurements. Figure 5 shows the UV-vis spectra of the series of particle assemblies before (b) and after (c) TBBT cross-linking, along with the corresponding solution-phase spectra (a). The red-shifting of the SP band positions, relative to that of the particles dissolved in solution (all near 510 nm), is again very obvious and similar to those observed earlier (Figure 3): for the particle thin films without the addition of TBBT,

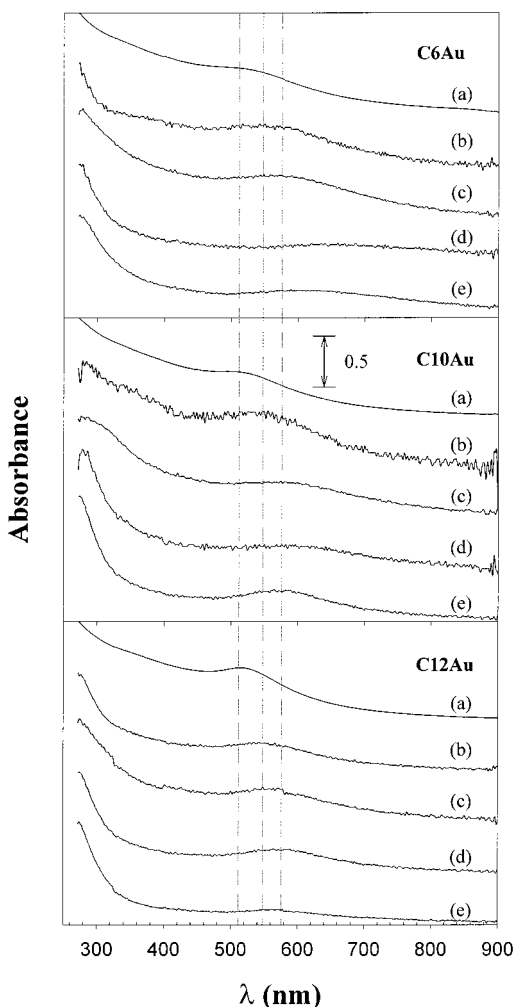


Figure 5. UV-vis spectra of varied gold nanoparticles deposited onto glass slide surfaces: (a) particles in solution, (b) particle monolayers without TBBT linkers and subsequent UVO exposure, (c) particle monolayers with TBBT linkers but without subsequent UVO exposure, (d) particle monolayers without TBBT linkers and after subsequent UVO exposure, and (e) particle monolayers with TBBT linkers and after subsequent UVO exposure. The experimental conditions were the same as those described in Figure 4. All spectra were normalized to their respective absorbance at 272 nm and offset for the sake of clarity.

the SP bands are typically found at 550 nm, whereas after TBBT cross-linking, the resulting particle assemblies exhibit the SP bands at even longer wavelength positions (ca. 580 nm).

The above studies clearly demonstrate that by strengthening the interparticle interactions through strong chemical linkages, the resulting particle assemblies exhibit significantly enhanced mechanical stability, compared to the LB thin films of nanoparticles without further chemical modifications. The interparticle spacing is found to be mainly determined by the molecular length of the rigid chemical bridges, regardless of the original thickness of the particle-protecting layers. The virtue of the approach described here is partly attributed to the diversity of surface decoration of the nanoparticle core surface, which might then be exploited in the fabrication of robust multifunctional stand-alone quantum dot thin films.

Surface Nanofabrications. The above-obtained robust particle superlattice networks might be useful for surface nanofabrication without involving sophisticated instrumentation. This nonlithographic approach is taking

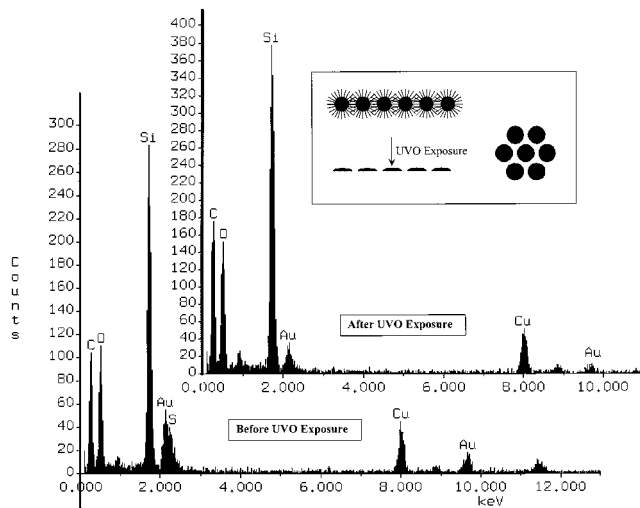


Figure 6. Energy-dispersive X-ray spectra of C12Au particle networks deposited on SiO_x -coated Cu grids before (Figure 4c) and after (Figure 4d) UVO exposure. The inset shows the schematic of the resulting gold quantum dot arrays after UVO treatment.

advantage of the easy fabrication of nanoparticle monolayers by LB deposition and the ready removal of simple organic molecules by photo-oxidation. The photosensitized cleaning protocol has been a common practice in surface science to remove organic contaminant molecules by the absorption of short-wavelength UV radiation. Here, we deposited the particle patches onto an optically stable substrate (e.g., glass slides, SiO_x -coated TEM grids, etc.), which was then subjected to UVO molecular cleaning to remove the organic components (mainly the alkane-thiolates and the TBBT linkers) and thus have the quantum arrays deposited onto the substrate surface.

Here, we take the C12Au particle networks as the illustrating example. Figure 4d shows the TEM micrograph of the same C12Au assemblies (Figure 4c) after the treatment of UVO cleaning for 15 min. One can see that although the superlattice ordering was disrupted somewhat, only a small number of particles were found to be coalesced and a rather large fraction of the particles were found to even maintain the hexagonal ordered structures. In addition, the average particle (cross-sectional) diameter was found to increase somewhat, from the original 5.1 nm to 6.1 nm after UVO exposure, suggesting that the particle shape might change from the original spherical morphology to a disklike island structure (Figure 6 inset). Alternatively, it might be due to the formation of gold oxide with a larger crystal lattice.

EDX analysis was carried out to examine the removal of the organic components. Figure 6 shows the spectra before and after the UVO treatment of the C12Au particle ensembles. One can see that the sulfur signal is virtually absent after UVO exposure, indicating the efficient desorption of the thiolates from the particle core surface; however, the carbon peak is still quite strong, most likely because of the deposition of carbon onto the metal quantum dot surfaces (the Cu, Si, and O peaks are from the TEM grids). A similar observation of carbon deposition was found with organic-capped Pt-Fe alloy particles that were thermally annealed at elevated temperatures.^{4a}

As the majority of the particles within the cross-linked networks are still well-separated in the superlattice matrix (Figure 4d), one would anticipate only very subtle variation of the optical responses of the resulting quantum dot arrays, as compared to those prior to the photo treatment.

Figure 3 (bottom panel) and Figure 5 (all d's and e's) show the UV-vis spectra of a series of gold particle networks after UVO exposure. One can see that after UV exposure, the TBBT-linked particle patches essentially demonstrate invariant absorption profiles (in particular, the SP energy; Figure 3 c2 and d2 and Figure 5 e's), consistent with the above TEM measurements (Figure 4c,d). In contrast, for the particle assemblies fabricated without the cross-linking of TBBT, after UVO exposure the absorption profiles (Figure 3 a2 and b2 and Figure 5 d's) are much broader and the SP band positions are mostly hard to locate. It is most likely that the latter is attributed to the coalescence of the particles upon UV and ozone excitation, considering the observed aggregation of particles even prior to the photo treatment (e.g., Figure 2a,b).

The resulting metal quantum dot arrays exhibit even stronger mechanical stability than the original cross-linked particle networks. For instance, it was found that the particle patches deposited onto a glass surface could be easily peeled off with a Scotch tape whereas the quantum dot arrays survived the tape test and stayed on the substrate surface without any visible damage.

In addition, by using other metal nanoparticles^{16c,20} one will anticipate that diverse surface nanostructures will be readily constructed, where the different chemical properties of the nanodots and the substrates might be exploited for nanoscale surface chemical patterning,

providing a complementary route to other surface decoration methods (e.g., surface nanografting¹⁴). Work toward this end is currently underway and will be reported in due course.

Conclusion

Long-range ordered and robust nanoparticle assemblies were fabricated by using the Langmuir-Blodgett method through interparticle cross-linking with bifunctional linkers. The protocol exploited the unique properties of nanoparticle surface functionalization by initiating surface exchange reactions between dithiol chemical bridges and nanoparticle-bound thiolate ligands at high surface pressures where ligand intercalation was possible. The obtained nanoparticle networks might be used in surface nanofabrication in a nonlithographic manner, leading to the construction of ordered arrays of metal quantum dots. It is anticipated that the protocols described here can be extended to other nanoparticle materials (e.g., other metal or semiconductor nanoparticles) and chemical bridges where diverse nanoparticle superlattice assemblies can be achieved.

Acknowledgment. The author is grateful to Dr. J.-B. Green (SIU) for providing access to the UVO cleaner. This work was supported by the Office of Naval Research and the SIU Materials Technology Center.

LA001728W

(20) Chen, S.; Huang, K.; Stearns, J. A. *Chem. Mater.* **2000**, *12*, 540.